

$\bar{\Lambda}/\bar{p}$ RATIOS IN HEAVY ION COLLISIONS AT 11.6 A · GeV/c

G. J. Wang, G. Welke, R. Bellwied, and C. Pruneau

*Department of Physics and Astronomy**Wayne State University, Detroit, MI 48202, U.S.A.**E-mail: welke@physics.wayne.edu*

We attempt to explain the $\bar{\Lambda}/\bar{p}$ ratios measured in heavy ion collisions at 11.6 A · GeV/c beam momentum within a hadronic framework. This ratio is enhanced relative to corresponding ratios in pp collisions, and is large when compared with thermal fits to heavy ion data. Using a detailed cascade calculation, we show that different annihilation cross-sections of $\bar{\Lambda}$'s and \bar{p} 's, and the net conversion of \bar{p} 's to $\bar{\Lambda}$'s, do not account for the enhancement in central collisions. For larger impact parameters, however, hadronic mechanisms may well suffice to produce the observed enhancement. Uncertainties in elementary cross-sections and formation times are considered.

I. INTRODUCTION

Anti-lambda ($\bar{\Lambda}$) cross-sections in heavy ion collisions are of interest because strangeness production is a potential signal for the formation of a quark-gluon plasma (QGP) in heavy ion collisions [1–3]. The ratio of anti-lambdas to anti-protons (\bar{p}) is of particular interest since it reflects the production of strange anti-quarks relative to non-strange light anti-quarks, and should increase substantially relative to the production expected from a superposition of NN collisions, if a QGP is formed.

Recent experiments have reported measurements of \bar{p} and $\bar{\Lambda}$ production in various heavy ion systems at the Brookhaven AGS and at the CERN SPS [4–8]. Experiment E859 reports the ratio of $\bar{\Lambda}$ and \bar{p} rapidity distributions to be $3 \pm 1 \pm 1$ in central Si+Pb collisions [4]. This ratio is corrected for finite experimental acceptance, efficiencies, and for \bar{p} creation from $\bar{\Lambda}$ decay (feed-down), and also takes into account that neutral $\bar{\Sigma}$ particles cannot be distinguished from the $\bar{\Lambda}$ sample. Experiment E864 has measured [5,6] the \bar{p} production cross-section in Au+Pb at 11.6 A · GeV/c. They compare this measurement with a similar one from the E878 collaboration that was obtained with a focusing spectrometer, and interpret the difference between the two measurements as an indicator of $\bar{\Lambda}$ production. E864 estimates that $\bar{\Lambda}/\bar{p} > 2.3$ at the 98% CL, with a most probable value of 3.5. At the SPS, NA35 has published $\bar{\Lambda}/\bar{p}$ ratios for pp , pA , S+S, S+Ag, and S+Au collisions at 200 A · GeV/c, and they observe a significant rise from 0.25 for pp -collisions to 1.5 for the heavy ion systems [7,8].

It is tempting to interpret the large reported ratios as evidence for the formation of a QGP: Many authors [9–11] have argued that the CERN multi-strange baryon ratios [12–14] can only be described by a QGP scenario. Moreover, in a systematic study of strangeness production in heavy ion collisions from SIS to SPS energy ranges, mostly based on kaon ratios, Geiss et al. [15] conclude that a QGP scenario is required to explain that data at AGS energies. This conclusion is, however, challenged by Au+Au RQMD simulations that find that the \bar{p} production cross-section appears to be lower than expected from the scaled NN \bar{p} cross-section.

Here we shall try to address quantitatively all possible hadronic contributions to the $\bar{\Lambda}/\bar{p}$ ratio using a cascade model [16]. We restrict calculations to AGS energies and show that “differential annihilation” of the two species and \bar{p} -to- $\bar{\Lambda}$ conversion processes can indeed enhance the $\bar{\Lambda}/\bar{p}$ ratio. We conclude that the effect is not large enough at central impact parameters, but may well suffice to explain the data from more peripheral events – thus hinting at a production mechanism outside of standard hadronic interactions.

We present our arguments as follows: Section II outlines a thermal model calculation with chemical equilibration and feed-down contributions. We fit the parameters of the model to rather liberal ranges of various kaon, pion and proton ratios measured in central Au+Au events, and show that the resulting $\bar{\Lambda}/\bar{p}$ ratio lies well below the E864 value. This conclusion has also been reached by other authors [17–19]. We consider transport simulations in the remainder of the paper, briefly describing the model [16] and discussing the relevant cross-sections in more detail. Actual measurements of the $\bar{\Lambda}$ and \bar{p} cross-sections [20,21] are used, rather than event generator parameterizations. Section IV presents our results, discussing also the uncertainties in the calculations, particularly those arising from the relatively poorly known $\bar{\Lambda}$ annihilation in the relevant energy range, and from particle formation times. We shall consider first central events, and then the more recent E864 results [22] at larger impact parameters. Speculative conclusions based on the quantitative discrepancy between calculations and the actual measurements at small impact parameters are presented in the last Section.

II. THERMAL MODEL

We consider in this Section a thermal model fit for Au+Au collisions at 11.6 GeV/c, at central impact parameters only. Our main motivation is to show that in such events the measured $\bar{\Lambda}/\bar{p}$ ratio is larger than predicted by a standard thermal model, even if we push the input fit ratios to extreme values.

The model is based on thermal and chemical equilibration up to some freeze-out, so that all relative abundances can be obtained from four parameters: the freeze-out temperature T_0 , the electric chemical potential μ_e , the baryonic chemical potential μ_b , and the strange chemical potential μ_s . Here,

$$\mu_i = q_i \mu_e + b_i \mu_b + S_i \mu_s$$

are particle chemical potentials, where q_i , b_i and S_i are the charge, baryon number and strangeness of species i , respectively. Note that the strange chemical potential is not fixed *a priori*. The distribution functions we use are for ideal Fermions and Bosons – we do not include mean fields or excluded volume modifications [23], which would alter our conclusions quantitatively, but not qualitatively. Of course, the final abundance of a particle is determined by both the primary number of this species at freeze-out, and by feed-down from heavier species after freeze-out. We include all mesons with rest mass ≤ 1 GeV/ c^2 , and all baryons with rest mass ≤ 1.7 GeV/ c^2 . We note that our final $\bar{\Lambda}$ numbers throughout include $\bar{\Sigma}^0$'s, as none of the experimental measurements can distinguish between the two species.

The results of the calculation are summarized in Table 1. The thermal fit parameters T_0 , μ_e , μ_b and μ_s are obtained by applying the conditions $|Q/B - 0.40| < 1\%$ and $|S| < 2\%$, where Q , B and S are the overall charge, baryon number and strangeness of the system, together with the constraints listed in Table 1. As motivated above, we purposefully choose rather large ranges in these latter constraints to show how difficult it would be to obtain the experimental $\bar{\Lambda}/\bar{p}$ ratio. The “errors” on the fitted values for T_0 and the chemical potentials listed in the caption of Table 1 indicate roughly the ranges that lead to results consistent with the constraint intervals.¹

While the agreement of most ratios with the data is relatively good (see Table 1, also Refs. [17,18]), we see that $\bar{\Lambda}/\bar{p} \lesssim 1.9$, at best, well below the 98% CL lower value of 2.3 reported by E864. In Figure 1 these results are illustrated graphically. Panel (a) shows $\bar{\Lambda}/\bar{p}$ as a function of the K^+/K^- ratio for various freeze-out temperatures T_0 . Large $\bar{\Lambda}/\bar{p} > 2$ result only if the freeze-out temperature and/or observed K^+/K^- ratio are pushed unreasonably high. A similar conclusion follows from Figure 1(b), which shows $\bar{\Lambda}/\bar{p}$ as a function of K^+/π^+ . In both panels the error bars/scatter points indicate values consistent with constraints not shown, and the dashed line represents the 98% lower CL of the E864 experiment.

Clearly, the experimental $\bar{\Lambda}/\bar{p}$ ratio has, at the very least, a significant non-thermal component: the lower experimental bound reported by E864 is larger than any reasonable thermal fit would allow.

III. CASCADE MODEL AND CROSS-SECTIONS

Generally, a thermal description is useful for a given particle species if its mean free path is small compared to the system size. This fact alone means that other approaches should also be investigated. We do so in the next Section, and discuss here the relevant cross-sections.

Our cascade model will be described in detail elsewhere [16], and we give here only a brief overview. It is used in this work to describe the evolution of the pions, kaons, and nucleons which act as a “background” for the \bar{p} and $\bar{\Lambda}$ species that interest us. The model is based on NN input data, and includes elastic and inelastic processes. For elastic collisions, resonance formation is considered if the energy and quantum numbers of the combined system are suitable. For inelastic collisions, we consider single diffractive processes, which effectively correspond to resonance production at low energies, and non-single diffractive processes, responsible for the remainder of the inelastic cross-section. All cross-sections are taken from experimental data whenever available, otherwise we use NN , πN or KN , and $\pi\pi$ or πK cross-sections for baryon-baryon, meson-baryon, and meson-meson interactions, respectively. Average particle numbers, the multiplicity distribution, and species abundances are also taken from data whenever available. For leading particles, the fractional longitudinal momentum is determined from a uniform distribution, while the transverse momentum is taken from $p_t \exp(-\beta p_t)$ with $\beta \approx 4.44$ (GeV/c)⁻¹. The transverse momenta of secondary

¹We note that these parameters are not inconsistent with overall energy conservation considerations.

particles are determined in a similar way, while their rapidities are chosen from a flat distribution. All conservation laws are strictly enforced.

The following processes are of particular importance for our discussion. Firstly, the production of \bar{p} 's and $\bar{\Lambda}$'s:

$$b_1 + b_2 \rightarrow N_1 + N_2 + B + \bar{B} (+\pi) \quad (1)$$

$$b + M \rightarrow N + B + \bar{B} (+\pi) \quad (2)$$

$$M + M \rightarrow B + \bar{B} (+\pi) \quad (3)$$

$$S^+ + S^- \rightarrow B + \bar{B} (+\pi) \quad (4)$$

$$b + S^+ \rightarrow b + \bar{B} + N (+K^+ + \pi) \quad (5)$$

$$M + S^+ \rightarrow N + \bar{B} (+S^+ + \pi) \quad (6)$$

Here, b represents a non-strange baryon, N a nucleon, B any baryon, M a light unflavored meson, and S^\pm a ± 1 -strangeness meson. We return to the question of production below. Secondly, in the same notation:

$$b + \bar{p} \rightarrow X \quad (7)$$

$$b + \bar{\Lambda} \rightarrow S^+ + \pi \quad (8)$$

$$\bar{b} + S^+ \rightarrow \bar{\Lambda} + \pi \quad (9)$$

$$\bar{p} + M \rightarrow \bar{\Lambda} + \pi + S^- \quad (10)$$

$$\bar{\Lambda} + M \rightarrow \bar{b} + S^+ (+\pi) \quad (11)$$

We refer to (7) and (8) as annihilation processes, and (9)–(11) as conversion processes. The inverse for all $2 \rightarrow 2$ body processes listed is also included, but we have not considered $3, 4, \dots \rightarrow 2$ detailed balance.

The experimental $p\bar{p}$ annihilation cross-section is well known, and can be parameterized as

$$\sigma_{p\bar{p}}^{annih}(p_{lab}) = 67 p_{lab}^{-0.7} \text{ mb} , \quad (12)$$

where p_{lab} is the momentum of the “beam” particle in GeV/ c with the “target” at rest. The solid line in Figure 2 shows this parameterization of the data (crosses). The $\bar{\Lambda}$ annihilation cross-section, on the other hand, is relatively poorly known, especially in the energy range we are interested in. We model it by assuming that the elastic cross-sections for $p\bar{\Lambda}$ and $p\Lambda$ are equal, and then use the data of Ref. [21] to obtain:

$$\sigma_{p\bar{\Lambda}}^{annih}(p_{lab}) = 15 (p_{lab}/10)^{-\alpha} \text{ mb} , \quad (13)$$

where the same comments apply as for Eq. (12). While the data is best fit by $\alpha = 0.5$, the uncertainty is rather large (see Figure 2; the diamonds are data from Ref. [21]). In fact, one might well argue that the $\bar{\Lambda}$ data is consistent with $\alpha = 0$, as shown by the dot-dashed line in Figure 2. We take $\alpha = 0$ as an extreme value that should lead to the greatest differential annihilation. For $\alpha = 0.7$, on the other hand, the $\bar{\Lambda}$ data is practically indistinguishable from the \bar{p} data. We shall subsequently investigate the behavior of $\bar{\Lambda}/\bar{p}$ with α .

The \bar{p} and $\bar{\Lambda}$ scattering with mesons is also an important process we need to consider. Broadly speaking, we have three types of collision: (1) thermalization of \bar{p} 's and $\bar{\Lambda}$'s through elastic collisions; (2) production of resonances that eventually decay back into \bar{p} 's or $\bar{\Lambda}$'s; and (3), most importantly, net conversion of \bar{p} 's to $\bar{\Lambda}$'s. Chief amongst these is

$$\bar{p} + K^+ \rightarrow \pi + \bar{\Lambda} \quad (\text{or resonances of } \bar{\Lambda}) , \quad (14)$$

for which we know the charge conjugate reaction to have a sizeable cross-section. The process (14) thus contributes to reducing the \bar{p} abundance while enhancing the $\bar{\Lambda}$ abundance in the final state. Given the pronounced strangeness enhancement in large systems such as Au+Au, the process (14) should be a relatively important piece of the $\bar{\Lambda}/\bar{p}$ “puzzle.”

The production rate of \bar{p} 's or $\bar{\Lambda}$'s is only $O(10^{-2})$ per event at the AGS, and cascade calculations are rather CPU intensive. We shall therefore perform an effective calculation of the survival probability by putting \bar{p} 's or $\bar{\Lambda}$'s in by hand, wherever and whenever a collision occurs in which the energy is sufficient for a $p\bar{p}$ or $\Lambda\bar{\Lambda}$ pair to be produced. Thus we assume that the pair production does not depend on energy, once above threshold, and take the relative initial production of \bar{p} 's and $\bar{\Lambda}$'s from pp data (see below). The presence of initial \bar{p} 's or $\bar{\Lambda}$'s is not permitted to influence the evolution of nucleons, pions and kaons – we restore particles that interacted with \bar{p} 's or $\bar{\Lambda}$'s to their pre-collision kinematics.

We may then calculate the $\bar{\Lambda}/\bar{p}$ ratio via the survival probabilities P_s and the number of converted anti-lambdas that survive, $\bar{\Lambda}^c$:

$$\frac{\bar{\Lambda}}{\bar{p}} \approx r_p \frac{P_s(\bar{\Lambda})}{P_s(\bar{p})} + 2r_c \frac{\bar{\Lambda}^c}{\bar{p}^s}, \quad (15)$$

where \bar{p}^s is the number of surviving \bar{p} 's. Here, $r_c \approx 0.25$ is a correction factor, as we overestimate $\bar{\Lambda}$ -production by assuming that all collisions of non-strange anti-baryons with positive strange mesons result in a $\bar{\Lambda}$. The factor two accounts for the conversion of \bar{n} 's to $\bar{\Lambda}$'s. Finally, r_p is the $\bar{\Lambda}/\bar{p}$ ratio in pp collisions. At $\sqrt{s} \sim 20$ GeV, it has a value [28–31] of 0.25–0.30. At AGS energies ($\sqrt{s} \sim 5$ GeV) its value is less established. Using Refs. [28–30], we infer a value of ~ 0.2 , but we shall use a value of $r_p \approx 0.25 + 0.0 - 0.1$ throughout this work. We note that mean field effects may very well reduce the effective r_p for in-medium production when compared [24] to the free space values. Our chosen value of r_p and error bars imply that the heavy ion $\bar{\Lambda}/\bar{p}$ ratios we obtain in subsequent calculations will be upper bounds.

IV. CASCADE CALCULATION: RESULTS

We begin by discussing the most central events, roughly 10% of the total cross-section. To illustrate the effect of differential annihilation versus net conversion, we show in Table 2 the different components of Eq. (15) for different α and $\tau = 0$ (no formation time) in central Au+Au simulation at AGS energies. For small α (small $\bar{\Lambda}$ annihilation cross-section), $\bar{\Lambda}/\bar{p}$ enhancement results almost entirely from differential annihilation. As α increases, the survival probability of a $\bar{\Lambda}$ and a \bar{p} become equal, and the sole enhancement in the final ratio results from conversion. Of course, as α increases the ratio $\bar{\Lambda}^c/\bar{p}^s$ decreases, since $\bar{\Lambda}^c$ refers to surviving anti-lambdas.

We show in Figure 3 the final $\bar{\Lambda}/\bar{p}$ ratios from cascade simulations (circles) for several values of α and τ , and for various systems, all at central impact parameters. The dashed lines show the E864 98% CL values for Au+Au. We clearly see that reducing the difference between $\bar{\Lambda}$ and \bar{p} annihilation, *i.e.*, increasing α , reduces the ratio (Figure 3 (a)-(c)). Similarly, a larger formation time τ also leads to a smaller ratio – the effective system size for annihilation and conversion is reduced as all particles require some time to be formed (see panel (d)). Moreover, for Au+Au, the maximum ratio obtainable (for $\alpha = 0$ and no formation time) lies at about the the E864 98% CL lower limit.

In discussing the results of Figure 3, we note that (1) realistic values for α are probably closer to 0.5 than 0.0; (2) formation times are probably not zero; and (3) our initial, *i.e.* pp $\bar{\Lambda}/\bar{p}$ ratio is probably an over-estimate, particularly in light of possible medium effects that penalize $\bar{\Lambda}$ production relative to \bar{p} production. This latter fact is reflected in the error bars for the ratio – our choice for $r_p = 0.25 + 0.0 - 0.1$ is what we consider an upper bound. We conclude that for central Au+Au events the most likely value of $\bar{\Lambda}/\bar{p}$ is most definitely $\lesssim 2$, and more likely somewhat below unity – smaller than the 98% CL reported by E864.

The $\bar{\Lambda}/\bar{p}$ ratio is larger in Si+Pb collisions than in Au+Au collisions in our calculation, but it is not a large effect (compare Figure 3 (a) and (c)). Within our model this difference has a simple geometric explanation: For Si+Pb, the \bar{p} 's and $\bar{\Lambda}$'s are produced close to the beam axis, leading to a larger average nuclear thickness that the anti-particle must traverse. Once again, though, realistic input parameter values of $\tau \sim 1$ and $\alpha \sim 0.4$ seem to suggest that our hadronic cascade misses the experimental lower bound of E859.

The solid lines in Figure 3 are results from a model calculation [32] that uses annihilation and net conversion mean free paths as an input to rate equations in a simplified geometric picture. Its only free parameter mocks up the effect of local matter expansion, local average momentum distributions, *etc.* It reproduces the trends in the data rather well.

Recently, E864 has also reported the impact parameter dependence of the $\bar{\Lambda}/\bar{p}$ ratio in Au+Au [22]. In Figure 4, the upper and lower solid line (drawn to guide the eyes) show the most probable (diamonds) and 98% CL (squares) values of these results, respectively. There are four centrality bins: From left to right they are $< 10\%$, $10\text{--}30\%$, $30\text{--}70\%$, and $> 70\%$ of the total cross-section, as obtained from transverse energy cuts. The short-dashed line joins cascade calculations (crosses) for $\alpha = 0$ and $\tau = 0$. Recall that both these parameters values are extreme: $\alpha = 0.4$ (box-crosses, joined by long dashes in Figure 4) is more likely, and does not reproduce the central data bin result. For larger impact parameters, however, we see that this conclusion is considerably weakened – the cascade result initially rises with increasing impact parameter to far above the data for $\alpha = 0$, while for $\alpha = 0.4$ it remains relatively flat, but eventually does intercept the experimental data in semi-central collisions.

Thus, while hadronic mechanisms seem inadequate for the most central events, we are not able to conclude with certainty that they fail to describe the data at larger impact parameters. We note that at higher energies the difference between the $\bar{\Lambda}$ and \bar{p} annihilation cross-section practically vanishes. Within the differential annihilation model, one might therefore predict (in hindsight) that $\bar{\Lambda}/\bar{p}$ at the SPS should be lower than at the AGS, as indeed observed, and indicating that the model has the correct beam-energy dependence.

V. CONCLUSIONS

The $\bar{\Lambda}/\bar{p}$ ratio in NN collisions at AGS energies is $\lesssim 0.25$, heavy ion experiments measure much larger values. A hadronic thermal model with chemical equilibration and feed-down contributions can only be pushed to values above 2 with much difficulty. For Au+Au, using the (unreasonable) extremes of $K^+/\pi^+ \sim 0.30$, $K^+/K^- \sim 6.0$, and $T_0 \sim 140$ MeV, we obtain an upper limit of $\bar{\Lambda}/\bar{p} \sim 2$, below the E864 98%–lower confidence limit of 2.3.

We have considered a non-equilibrium description, and presented results from a detailed cascade calculation. Chief inputs to our calculations are the $\bar{\Lambda}$ and \bar{p} annihilation cross-sections with nucleons, as well as processes that convert \bar{p} 's into $\bar{\Lambda}$'s. The $\bar{\Lambda}$ annihilation cross-section is relatively poorly known in the relevant energy range, but it may be argued that it is somewhat less than \bar{p} annihilation at AGS energies. Our parameter α controls this difference, with $\alpha = 0$ corresponding to the greatest difference, and $\alpha = 0.7$ corresponding to a cross-section that is practically indistinguishable from \bar{p} annihilation. Currently, the cross-section data is (“best”) fit by $\alpha = 0.5$. Another important input is the cross section of NN $\bar{\Lambda}$ to \bar{p} production, which in our calculation may well be an overestimate, compared to free NN data and also in view of medium effects on the particle production. Our asymmetric error bars on the input NN ratio reflect this recognition.

In Au+Au cascade simulations for small impact parameters at AGS energies, the largest $\bar{\Lambda}/\bar{p}$ ratio obtainable is $\sim 2.4 + 0.2 - 1.0$, for a flat and small $\bar{\Lambda}$ annihilation cross-section ($\alpha = 0$) and no formation time ($\tau = 0$). Both these input values are extreme. What we currently believe to be more reasonable inputs lead to a value of $\bar{\Lambda}/\bar{p} \lesssim 1$ (~ 1 for Si+Pb), far below the lower bound of the E864 experiment. The model essentially fails to describe the ratio. For larger impact parameters, however, we cannot conclude with certainty that the hadronic mechanisms are inadequate in describing the data. While the data drops dramatically as the impact parameter increases, the calculation remains relatively flatter, and even rises somewhat for an energy independent $\bar{\Lambda}$ annihilation cross-section.

In conclusion, the large $\bar{\Lambda}/\bar{p}$ ratios in central Au+Au collisions at 11.6 A · GeV/c are not easily explained by hadronic mechanisms. This is no longer true at larger impact parameters, and it is interesting to speculate if QGP formation in central events might be a possible explanation. Of course, more accurate measurements of the $\bar{\Lambda}$ annihilation cross-section in the relevant energy range are needed, as well as a better understanding of hadronic medium effects in $\bar{\Lambda}$ and \bar{p} production and annihilation, before any more definite conclusion can be reached.

Acknowledgments: Gerd Welke acknowledges useful discussions with Pawel Danielewicz, Jörg Aichelin and Wolfgang Cassing. GW and G. Wang acknowledge the hospitality of the Institute for Nuclear Theory, Seattle, where this work was completed. This work was supported in part by the U.S. Department of Energy under Grant No. DE-FG02-93ER40713.

VI. REFERENCES

1. E.V. Shuryak, *Phys. Rep.* 115:151 (1984).
2. P. Koch et al., *Phys Rep.* 142:167 (1986).
3. J. Rafelski, *Phys. Rep.* 88:331 (1982).
4. G.S.F. Stephans and Y. Wu for the E859 Coll., *J. Phys. G* 23:1895 (1997)
5. T.A. Armstrong et al., *Phys. Rev. Lett.* 79:3351 (1997).
6. J. Lajoie for the E864 Coll., Antiproton production in 11.5 A · GeV/c Au+Pb nucleus collisions, *in*: “HIPAGS 96,” *ibid.*, p. 59.
7. D. Röhrich for the NA35 Coll., STRANGENESS 96, Budapest, May 96
8. J. Günther for the NA35 Coll., *Nucl. Phys.* A590:487c (1995).
9. J. Letessier et al., *Phys. Rev.* D51:3408 (1995).
10. J. Letessier, *Nucl. Phys.* A590:613c (1995).
11. J. Sollfrank et al., *Z. Phys.* C61:659 (1994).
12. E. Judd for the NA36 Coll., *Nucl. Phys.* A590:291c (1995).
13. D. Dibari for the WA85 Coll., *Nucl. Phys.* A590:307c (1995).

14. J.B. Kinson for the WA97 Coll., *Nucl. Phys.* A590:317c (1995).
15. J. Geiss, W. Cassing, and C. Greiner, LANL preprint nucl-th/9805012 (1998).
16. G.J. Wang, and G. Welke, to be published.
17. P. Braun–Munzinger et al., *Phys. Lett.* B344:43 (1995).
18. P. Braun–Munzinger et al., *Phys. Lett.* B365:1 (1996).
19. E. Schnedermann, and U. Heinz, *Phys. Rev.* C50:1675 (1994).
20. S. Gjesdal et al., *Phys. Lett.* B40:152 (1972).
21. F. Eisele et al., *Phys. Lett.* B60:297 (1976); B60:1067 (1976), and references therein.
22. C.A. Pruneau for the E864 Coll., Strangelet Searches, Light Nuclei, and p-bar Production Measurements by AGS E864, *in*: “Proceedings of the Quark Matter ‘97 Conference,” December 1–5, 1997, Tsukuba, Japan; to appear in *Nucl. Phys. A*.
23. J. Cleymans, and H. Satz, *Z. Phys.* C57:135 (1993).
24. W. Cassing, and E.L. Bratkovskaya, Hadronic and electromagnetic probes of hot and dense nuclear matter, Universität Giessen (1998), to appear in *Physics Reports*.
25. M. Gonin for the E802 Coll., Meson production from the E802 and E866 experiments at the AGS, *in*: “Heavy–Ion Physics at the AGS: HIPAGS 93,” G. Stephans, S. Steadman, and W. Kehoe eds., MIT Laboratory for Nuclear Science, Cambridge (1993) p. 184 .
26. H. Sako for the E866 Coll., Antiproton production in 11.7 A · GeV/*c* Au+Au collisions from E866, *in*: “HIPAGS 96,” *ibid.*, p. 67.
27. J. Lajoie (E864 Collab.), private communication.
28. V. Blobel et al., *Nucl. Phys.* B69:454 (1974).
29. M. Antinucci et al., *Lett. Nuovo Cim.* 6:121 (1973).
30. J. Whitmore, *Phys. Rep.* 10:273 (1974).
31. M. Gaździcki, and D. Röhrich, *Z. Phys.* C71:55 (1996).
32. G.J. Wang, R. Bellwied, C. Pruneau, and G. Welke, Anti-Lambda/Anti-Proton Ratios at the AGS, *in*: Proceedings of the 14th Winter Workshop on Nuclear Dynamics, Snowbird, Utah, 31 January – 6 February 1998, “Advances in Nuclear Dynamics 4,” W. Bauer and H.G. Ritter, eds. (Plenum Publishing, 1998).

VII. TABLES

TABLE 1. Thermal and experimental particle ratios for central Au+Au collisions at 11.6 GeV/c. The parameter ranges are $T_0 = 120 \pm 14$ MeV, $\mu_b = 556 \pm 19$ MeV, $\mu_s = 111 \pm 14$ MeV, and $\mu_e = -14 \pm 2$ MeV. The second column lists the range of the various constraint ratios considered.

Ratio	Constraint Range	Thermal Model	Data		
			Ratio	Rapidity	Ref.
K^+/π^+	0.16–0.28	0.23 ± 0.03	0.22 ± 0.01	0.5–1.3	[25]
K^+/K^-	4.0–6.0	4.73 ± 0.53	5.0 ± 1.0	0.5–1.3	[25]
K^-/π^-	–	$(3.50 \pm 0.62) \times 10^{-2}$	0.028	1.2–2.0	[26]
π^+/p	0.6–1.2	0.71 ± 0.09	–	–	–
π^-/p	0.8–1.4	1.00 ± 0.10	1.00	1.2–2.0	[26]
Λ/p	–	0.16 ± 0.02	–	–	–
\bar{p}/p	–	$(3.48 \pm 3.44) \times 10^{-4}$	$(5 \pm 2) \times 10^{-4}$	1.6 ($p_\perp \sim 0$)	[27]
$\bar{\Lambda}/\bar{p}$	–	1.58 ± 0.30	3.5	1.6 ($p_\perp \sim 0$)	[6]
			> 2.3 (98% CL)	1.6 ($p_\perp \sim 0$)	[6]

TABLE 2 Survival probabilities P_s , the ratio of surviving converted $\bar{\Lambda}^c$'s to surviving \bar{p}^s , and final $\bar{\Lambda}/\bar{p}$ ratio for various α and $\tau = 0$ fm/c, in central ($\lesssim 10\%$) Au+Au cascade simulations.

α	$P_s(\bar{\Lambda})$ (%)	$P_s(\bar{p})$ (%)	$\bar{\Lambda}^c/\bar{p}^s$	$\bar{\Lambda}/\bar{p}$
0.0	12.1 ± 0.3	1.5 ± 0.1	0.75 ± 0.07	$2.4+0.2-1.0$
0.2	6.0 ± 0.2	1.5 ± 0.1	0.45 ± 0.06	$1.2+0.1-0.5$
0.4	3.3 ± 0.2	1.5 ± 0.1	0.38 ± 0.06	$0.7+0.1-0.3$
0.7	1.5 ± 0.05	1.5 ± 0.1	0.16 ± 0.02	$0.3+0.04-0.1$

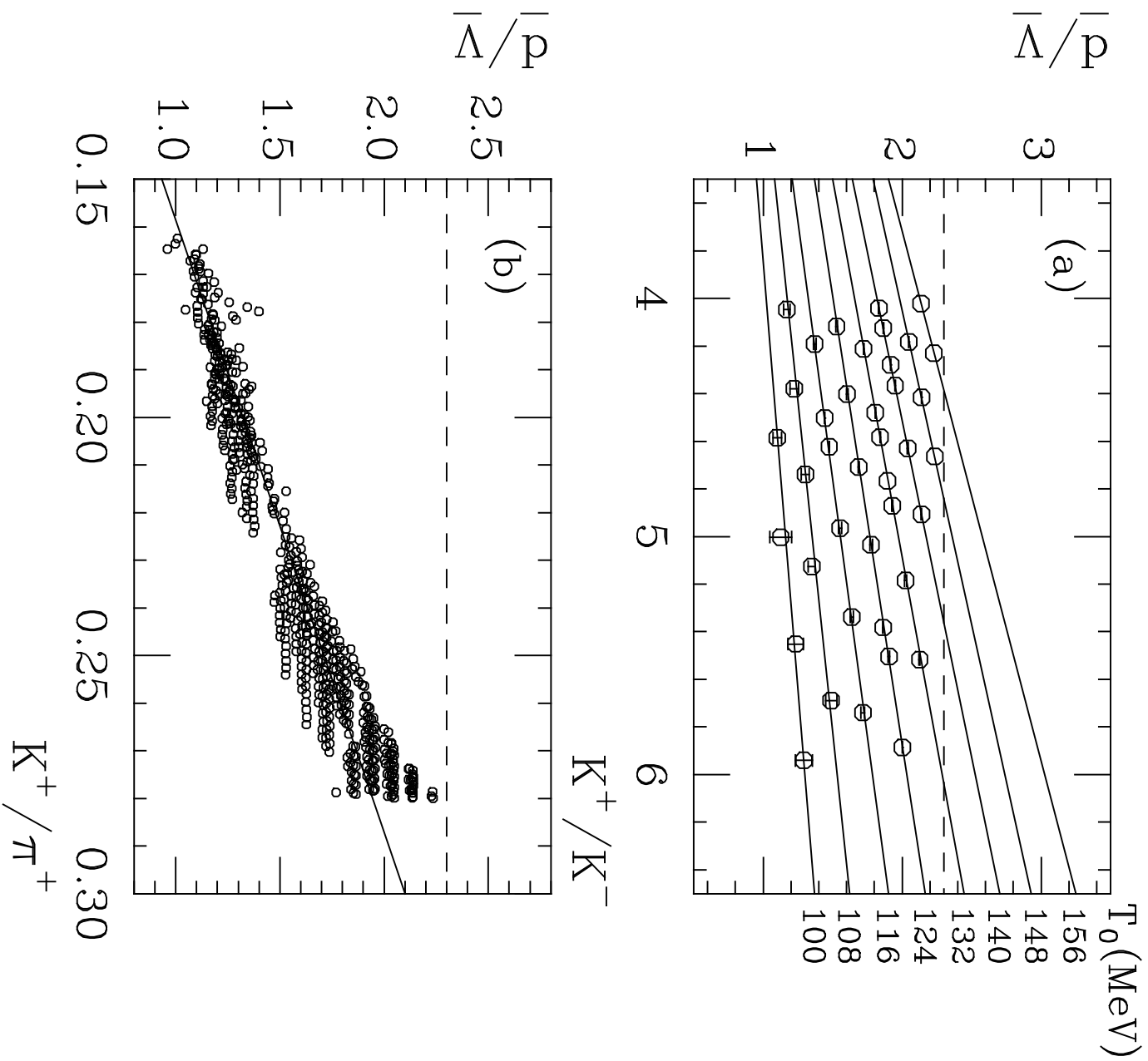
VIII. FIGURE CAPTIONS

FIGURE 1. (a) Thermal $\bar{\Lambda}/\bar{p}$ ratios as a function of K^+/K^- for various freeze-out temperatures T_0 . (b) Thermal $\bar{\Lambda}/\bar{p}$ ratios as a function of K^+/π^+ . The error bars/scatter points indicate values consistent with constraints not shown (see Table 1 for details). The solid lines are to guide the eye only; the dashed line represents the 98% lower CL of the E864 measurements.

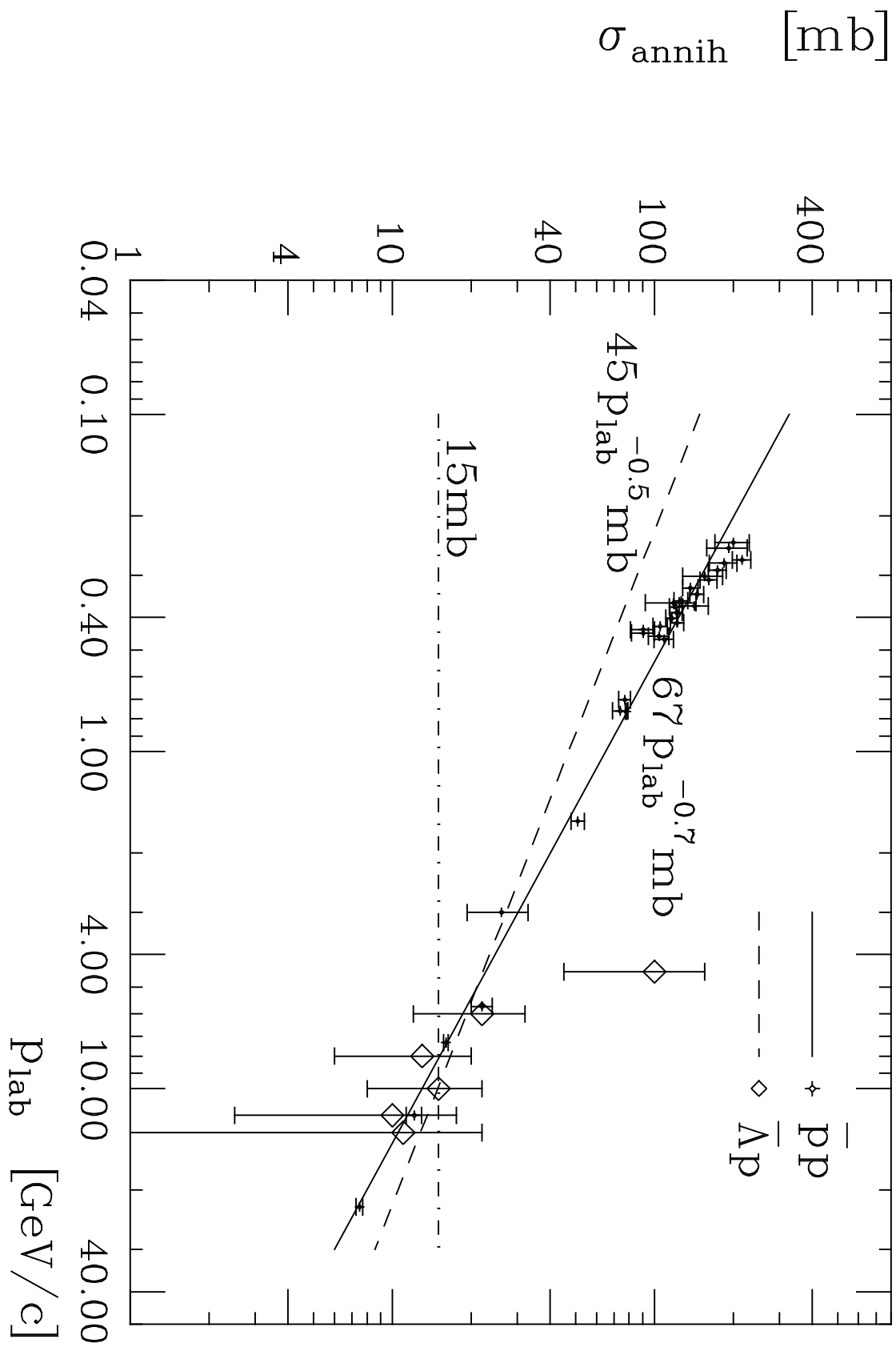
FIGURE 2. The annihilation cross-sections of \bar{p} ($\bar{\Lambda}$) with nucleons, as a function of the incident momentum of the \bar{p} ($\bar{\Lambda}$). The solid and dashed lines are fits to the \bar{p} and $\bar{\Lambda}$ data, respectively, while the dot-dashed curve is the extreme fit to the $\bar{\Lambda}$ data (with $\alpha = 0$ in Eq. (13)). The $\bar{\Lambda}$ data (diamonds) are from Ref. [21].

FIGURE 3. $\bar{\Lambda}/\bar{p}$ ratios calculated in the cascade model, for various values of α , and τ for central Si+Pb and Au+Au collisions. The solid lines are results of a geometric model calculation of Ref. [32], while the dashed lines show the E864 lower 98% CL [6].

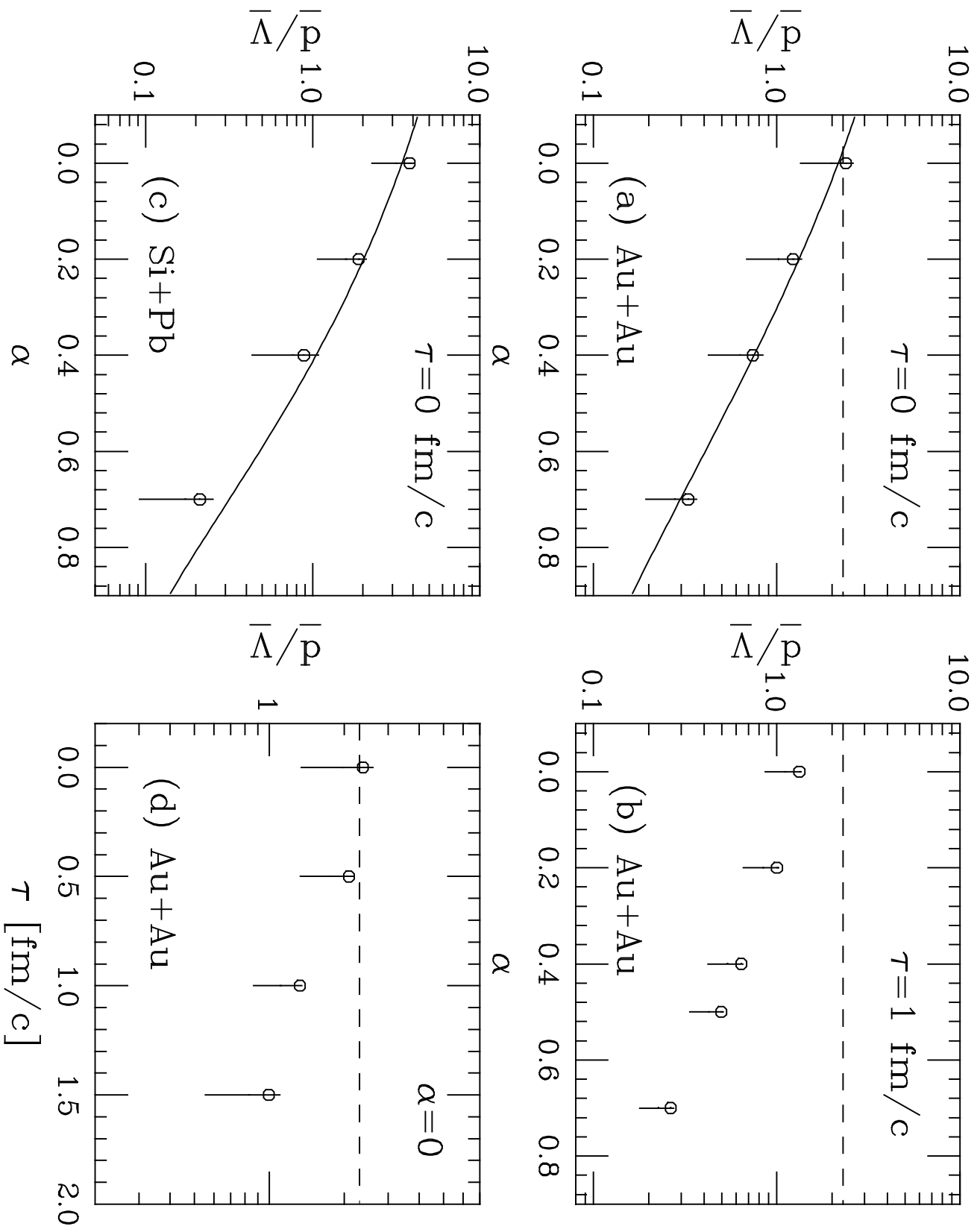
FIGURE 4. $\bar{\Lambda}/\bar{p}$ ratios as a function of centrality for Au+Au and zero formation time τ . All lines are drawn to guide the eye only. The upper solid line shows the E864 most probable values, the lower solid line represents the E864 98% CL [6,22]. The crosses are cascade calculations for $\alpha = 0$, while the cross-box points are for $\alpha = 0.4$. Some points are offset slightly to clarify the error bars.

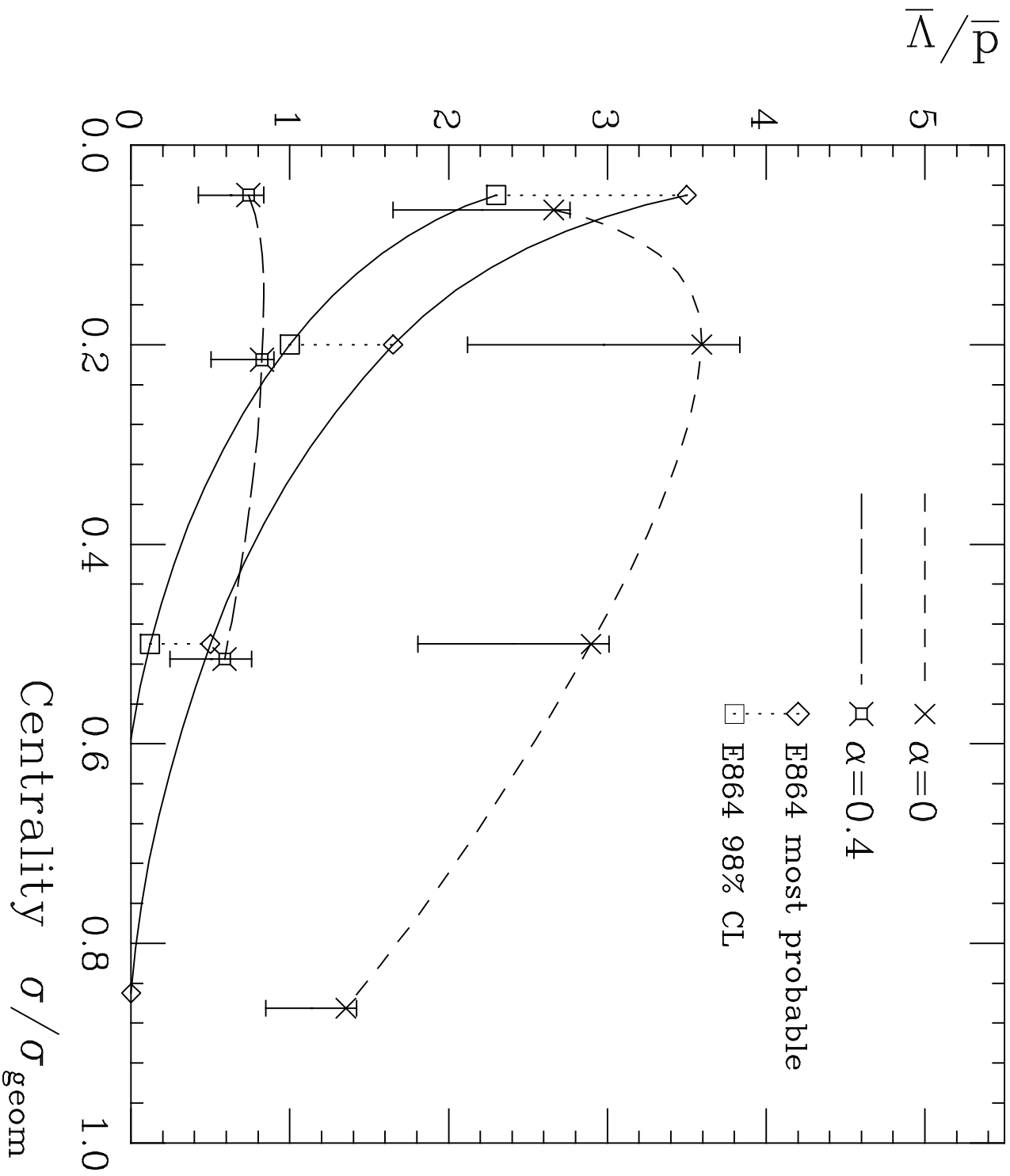


Wang et al, Figure 1



Wang et al, Figure 2





Wang et al, Figure 4